

1 **Loss of Tuberous Sclerosis Complex 2 sensitizes tumors to nelfinavir-**  
2 **bortezomib therapy to intensify endoplasmic reticulum stress induced cell**  
3 **death**

4

5 Charlotte E. Johnson<sup>1\*</sup>, Elaine A. Dunlop<sup>1\*</sup>, Sara Seifan<sup>1</sup>, Henry D. McCann<sup>1</sup>, Trevor Hay<sup>2</sup>,  
6 Geraint J. Parfitt<sup>2</sup>, Ashley T. Jones<sup>1</sup>, Peter J. Giles<sup>1</sup>, Ming H. Shen<sup>1</sup>, Julian R. Sampson<sup>1</sup>, Rachel  
7 J. Errington<sup>1</sup>, D. Mark Davies<sup>1,3</sup>, Andrew R. Tee<sup>1</sup>

8 <sup>1</sup>Division of Cancer and Genetics, Cardiff University, Heath Park, Cardiff, CF14 4XN, UK.

9 <sup>2</sup>European Cancer Stem Cell Research Institute, Cardiff University, Hadyn Ellis Building,  
10 Maindy Road, Cardiff, CF24 4HQ.

11 <sup>3</sup>Department of Oncology, South West Wales Cancer Centre, Singleton Hospital, Swansea,  
12 SA2 8QA.

13

14 \*C.E.Johnson and E.A.Dunlop contributed equally to this work.

15

16 **Corresponding author:** Dr. Andrew R. Tee, Division of Cancer and Genetics, Cardiff  
17 University, Cancer Genetics Building, 1st Floor, Heath Park, Cardiff, CF14 4XN, UK.

18 Telephone number: +44 (0)2920 687856, Fax: +44 (0)2920 746551, e-mail address:  
19 [teea@cardiff.ac.uk](mailto:teea@cardiff.ac.uk)

20

21 **Running title:**

22 Nelfinavir-bortezomib selectively kill TSC2-deficient cells

23

24 **Financial Support:**

25 This work was supported by Health and Care Research Wales (the Wales Cancer Research  
26 Centre) (to ED, AT, PG and TH), the Tuberous Sclerosis Association (to ED, AT and MS),  
27 Cancer Research Wales (to CJ, RJE and AT), the Tuberous Sclerosis Alliance (to ED and AT)  
28 and BBSRC (to RJE).

29

30

31

32

33

34

35

36

37 **Abbreviations:** AMPK (AMP-activated protein kinase), ANOVA (analysis of variance), ATF4  
38 (activating transcription factor 4), BiP (binding immunoglobulin protein), BTZ (bortezomib),  
39 CASP (caspase), CHOP (C/EBP homologous protein), CI (combination index), ddCT (delta-  
40 delta threshold cycle), DMEM (Dulbecco's modified Eagle's medium), DMSO (dimethyl  
41 sulfoxide), DTT (dithiothreitol), ELT3 (Eker rat leiomyoma-derived cells), ER (endoplasmic  
42 reticulum), ERO1L (endoplasmic reticulum oxidoreductase 1 alpha), ETO (etoposide), FBS  
43 (foetal bovine serum), GADD34 (growth arrest and DNA damage-inducible protein 34),  
44 GATOR (GTPase-activating protein activity toward RAGs), HSPA5 (heat shock protein family  
45 A [HSP70] member 5), IMPACT (impact RWD domain protein), IRE1 $\alpha$  (inositol-requiring and  
46 ER-to-nucleus signaling protein 1 $\alpha$ ), K-RAS (KRAS Proto-Oncogene, GTPase), MEF (mouse  
47 embryonic fibroblast), mTORC1 (mammalian/mechanistic target of rapamycin complex 1),  
48 NFV (nelfinavir), PARP (poly[ADP-ribose] polymerase), PBS (phosphate buffered saline),  
49 PERK (PRKR-like endoplasmic reticulum kinase), PPI (protein phosphatase 1), PTEN  
50 (Phosphatase And Tensin Homolog), RAP (rapamycin), RIPA (radio immunoprecipitation  
51 assay), RPMI (Roswell Park Memorial Institute), SD (standard deviation), SESN2 (sestrin 2),  
52 TPG (thapsigargin), TRIB3 (tribbles homologue 3), TS (tuberous sclerosis), TSC (tuberous  
53 sclerosis complex), UPR (unfolded protein response), XBP1 (X-box binding protein 1).

54

## 55    **Abstract**

56    Cancer cells typically lose homeostatic flexibility because of mutations and dysregulated  
57    signaling pathways involved in maintaining homeostasis. Tuberous Sclerosis Complex 1  
58    (TSC1) and TSC2 play a fundamental role in cell homeostasis, where signal transduction  
59    through TSC1/TSC2 is often compromised in cancer, leading to aberrant activation of  
60    mechanistic target of rapamycin complex 1 (mTORC1). mTORC1 hyperactivation increases  
61    the basal level of endoplasmic reticulum (ER) stress via an accumulation of unfolded protein,  
62    due to heightened *de novo* protein translation and repression of autophagy. We exploit this  
63    intrinsic vulnerability of tumor cells lacking TSC2, by treating with nelfinavir to further  
64    enhance ER stress while inhibiting the proteasome with bortezomib to prevent effective  
65    protein removal. We show that TSC2-deficient cells are highly dependent on the  
66    proteosomal degradation pathway for survival. Combined treatment with nelfinavir and  
67    bortezomib at clinically relevant drug concentrations show synergy in selectively killing  
68    TSC2-deficient cells with limited toxicity in control cells. This drug combination inhibited  
69    tumor formation in xenograft mouse models and patient-derived cell models of TSC and  
70    caused tumor spheroid death in 3D culture. Importantly, 3D culture assays differentiated  
71    between the cytostatic effects of the mTORC1 inhibitor, rapamycin and the cytotoxic effects  
72    of the nelfinavir/bortezomib combination. Through RNA sequencing, we determined that  
73    nelfinavir and bortezomib tip the balance of ER protein homeostasis of the already ER-  
74    stressed TSC2-deficient cells in favour of cell death. These findings have clinical relevance in  
75    stratified medicine to treat tumors that have compromised signaling through TSC and are  
76    inflexible in their capacity to restore ER homeostasis.

## 77    **Keywords:**

78    Nelfinavir; Bortezomib; Cancer; mTOR; ER stress

79

80

## 81    **1. Introduction**

82    Cancer cells often exhibit enhanced endoplasmic reticulum (ER) stress, due to a combination  
83    of inappropriately activated protein synthesis, high mutational load, oxidative stress and  
84    relative nutrient depletion that leads to the accumulation of misfolded protein [1]. The  
85    unfolded protein response (UPR) pathway restores ER homeostasis by three main  
86    mechanisms; by slowing the rates of global protein translation, by targeting unfolded  
87    protein to proteolytic degradation pathways (such as through autophagy and the  
88    proteasome), and through enhancement of protein folding orchestrated by molecular  
89    protein chaperones within the ER. If the UPR fails to restore the ER protein folding  
90    environment in a timely manner, cell death will ensue.

91 Mechanistic target of rapamycin (mTOR) (also referred to as mammalian target of  
92 rapamycin) orchestrates cell growth control by functioning as a key regulator of protein  
93 translation. Hyperactivation of mTOR complex 1 (mTORC1) is known to elevate the basal  
94 levels of ER stress through inappropriately high levels of protein synthesis and an  
95 accumulation of unfolded protein [2]. Aberrant signal transduction through mTORC1 can  
96 also potentially repress autophagy (reviewed in [3]). When autophagy is compromised, the  
97 proteasome becomes the primary proteolytic pathway to clear unfolded protein aggregates  
98 from the cell, thereby restoring ER homeostasis and preventing cell death [4].

99 Inactivating mutations in either Tuberous Sclerosis Complex 1 (*TSC1*) or *TSC2* give rise to  
100 Tuberous Sclerosis (TS), a genetic disorder where patients are predisposed to mTORC1-  
101 dependent tumor growth in various organs including the brain, kidney, eyes, lung, heart,  
102 and skin (for review see [5]). Functional loss of *TSC2* and resulting activation of mTORC1 was  
103 shown to upregulate the proteasome [6]. We hypothesise that mTORC1-driven cancers have  
104 an increased dependency on the proteasome for survival in response to ER stress.  
105 Therefore, a feasible therapeutic strategy might be to inhibit the proteasome with the aim  
106 to increase ER stress beyond a tolerated survival threshold. In support of this concept,  
107 selective cytotoxicity of proteasome inhibitors has been shown in cancer cell models with  
108 heightened mTORC1 signaling [7,8]. However, the proteasome inhibitor, bortezomib, had  
109 little efficacy as a single agent in preventing renal cystadenoma development *in vivo* in a  
110 *Tsc2*<sup>+/-</sup> mouse model [9]. This study suggested that targeting the proteasome alone is  
111 unlikely to cause cytotoxicity in mTORC1-active tumors. We therefore examined the effects  
112 of targeting the proteasome with bortezomib in combination with nelfinavir. Nelfinavir was  
113 originally used as a HIV protease inhibitor but has shown activity against a broad range of  
114 cancer models. One of its proposed mechanisms of anti-cancer action is via induction of ER  
115 stress [10]. Bortezomib has enhanced activity against advanced haematological  
116 malignancies such as multiple myeloma, recurrent multiple myeloma and mantle cell  
117 lymphoma when combined with nelfinavir and this combination is well tolerated in patients  
118 [11]. Combined nelfinavir and bortezomib therapy is cytotoxic to breast cancer, acute  
119 myeloid leukaemia, non-small cell lung cancer and myeloma cancer models [12,13,14],  
120 prompting several clinical trials (ClinicalTrials.gov: NCT01164709, NCT02188537,  
121 NCT01555281).

122 In an effort to stratify therapy, we wanted to determine whether specific inactivation of  
123 *TSC2*, a key regulator of mTORC1, would sensitise cell and tumor models to combined  
124 nelfinavir and bortezomib treatment. Previously we showed that combined treatment with  
125 nelfinavir and the autophagy inhibitor, chloroquine, was sufficient to kill *TSC2*-deficient cell  
126 lines or cancer cells with a high level of mTORC1 signal transduction and ER stress burden  
127 [15]. In this study, using both *in vitro* and *in vivo* mTORC1-hyperactive tumor models, we  
128 reveal that mTORC1-hyperactive cell lines and tumors are sensitive to combination  
129 nelfinavir and bortezomib induced cytotoxicity mediated through ER stress, while normal  
130 cells are able to tolerate this drug combination through intact compensatory mechanisms.



## 2. Results

### **2.1. ER stress is elevated upon combined treatment with nelfinavir and bortezomib in *Tsc2*<sup>-/-</sup> MEFs.**

To assess ER stress induction after combined nelfinavir and bortezomib treatment, we analysed downstream ER stress markers by western blotting. As a control we employed MG132 to inhibit the proteasome. Nelfinavir and bortezomib individually enhanced the level of ER stress in *Tsc2*<sup>-/-</sup> MEFs, as shown by increases in ATF4, CHOP and GADD34 protein levels, while induction of ATF4, CHOP and GADD34 in *Tsc2*<sup>+/+</sup> MEFs was less evident (Figure 1A). Combined nelfinavir and bortezomib treatment further elevated the protein levels of ATF4, CHOP and GADD34 compared to single drug treatment, particularly in *Tsc2*<sup>-/-</sup> MEFs.

We next analysed *Xbp1* mRNA splicing, which is a functional readout of ER stress and IRE1 $\alpha$  activation. Thapsigargin was employed as a control drug to induce ER stress. We observed more *Xbp1* mRNA splicing upon nelfinavir treatment in both the *Tsc2*<sup>+/+</sup> and *Tsc2*<sup>-/-</sup> MEFs. Bortezomib treatment did not result in *Xbp1* mRNA splicing as a single agent and did not further enhance the splicing of *Xbp1* mRNA when combined with nelfinavir (Figure 1B). To confirm this differential ER stress induction between cells with and without *Tsc2*, we examined the mRNA levels of *Chop* and *Bip* (Figure 1C). In untreated cells, both the *Chop* and *Bip* mRNA in *Tsc2*<sup>-/-</sup> MEFs were 5-fold and 2-fold higher, respectively, when compared to *Tsc2*<sup>+/+</sup> MEFs, indicating that ER stress is basally elevated in *Tsc2*<sup>-/-</sup> MEFs. The *Tsc2*<sup>-/-</sup> MEFs were particularly sensitive to nelfinavir treatment (either as a single agent or in combination with bortezomib), resulting in a 2.5 – 3.3-fold higher level of *Chop* expression and a 1.8 – 2.2-fold higher level of *Bip* expression when compared to the *Tsc2*<sup>+/+</sup> cells. Bortezomib also induced a 3-fold increase in *Chop* mRNA and a 2.4-fold increase in *Bip* mRNA in the *Tsc2*<sup>-/-</sup> cells compared to the control cells. These data demonstrate that both nelfinavir and bortezomib treatment induce a higher ER stress burden in cells lacking *Tsc2*. To examine whether drug treatment was inducing CHOP via the PERK pathway, we employed a PERK inhibitor, GSK2606414 (Figure 1D). CHOP expression induced by nelfinavir and bortezomib was markedly repressed with GSK2606414, revealing that these drugs are inducing an ER stress response through PERK.

Given that bortezomib promotes ER stress via proteasomal inhibition and that nelfinavir has also been reported to inhibit the proteasome [16], we examined proteasome activity through either detection of polyubiquitinated protein (Figure 1A), or levels of chymotrypsin-like activity (Figure 1E) after drug treatment. As expected, treatment with bortezomib alone, or in combination, greatly enhanced the levels of polyubiquitinated protein and effectively reduced chymotrypsin-like activity, indicating robust proteasome inhibition. At 20  $\mu$ M, nelfinavir did not show proteasome inhibition in either assay.

Elevation of protein synthesis by mTORC1 hyperactivation likely drives ER stress in *Tsc2*-deficient cells, but has not been examined to date. We analysed *de novo* protein synthesis

using pulse-chase [<sup>35</sup>S]-methionine labelling experiments of *Tsc2*<sup>-/-</sup> and wild-type control cells in the presence or absence of nelfinavir and bortezomib (Figure 1F). We observed that the *Tsc2*<sup>-/-</sup> cells had almost 4-fold elevation of protein synthesis compared to wild-type, showing that basally ER stressed *Tsc2*<sup>-/-</sup> cells maintain a high level of protein synthesis. After 6 h of nelfinavir and bortezomib dual treatment, protein translation was markedly reduced.

## **2.2. Proteasome inhibition induced death of *Tsc2* deficient cells which is enhanced by nelfinavir.**

We speculated that combined nelfinavir and bortezomib treatment might selectively induce cell death in *Tsc2*<sup>-/-</sup> MEFs compared to *Tsc2*<sup>+/+</sup> MEFs. We quantified cell death by flow cytometry with DRAQ7 labelling (Figures 2A and 2B). DRAQ7 is a membrane impermeable far-red fluorescent DNA-binding dye that measures cell death via increased membrane permeability. Both MG132 and bortezomib as single agents caused selective cell death in the *Tsc2*<sup>-/-</sup> MEFs but not in *Tsc2*<sup>+/+</sup> MEFs, revealing that cells devoid of *Tsc2* are dependent on the proteasome for their survival. Combined treatment of nelfinavir with bortezomib enhanced cell death in the *Tsc2*<sup>-/-</sup> MEFs (83.2% ± 9.2 cell death), with minimal toxicity observed in the *Tsc2*<sup>+/+</sup> MEFs (17.5% ± 7.7). The low level of cell death in the *Tsc2*<sup>+/+</sup> MEFs is not significantly different to the DMSO vehicle control. A similar pattern was observed for the nelfinavir/MG132 combination. To validate these findings, we utilised *Tsc2*-deficient and re-expressing ELT3 rat smooth muscle cells [17]. These results mirrored that seen in the *Tsc2*<sup>-/-</sup> MEFs (Supplementary Figure 1A and 1B).

To further examine cell death in *Tsc2*<sup>-/-</sup> MEFs we quantified DNA fragmentation after treatment (Figure 2C). We observed significant induction of DNA fragmentation after bortezomib treatment, which was further enhanced when combined with nelfinavir. No DNA fragmentation was evident with nelfinavir treatment alone. We next analysed several apoptosis markers by western blot (Supplementary Figure 1C). We observed cleavage of caspase8, caspase 3 and PARP in *Tsc2*<sup>-/-</sup> MEFs upon treatment with bortezomib alone or co-treatment with nelfinavir and proteasome inhibitors, whilst no marked cleavage was observed in wild-type cells. We could partially but significantly rescue *Tsc2*<sup>-/-</sup> MEFs from nelfinavir/bortezomib-induced cell death by inhibiting apoptosis with the pan caspase inhibitor, Z-VAD-FMK, suggesting cell death is partly mediated through caspase activation (Figure 2D).

To determine whether other sporadic cancer cell lines were also sensitive to combined nelfinavir and bortezomib treatment, we examined human NCI-H460 lung cancer and HCT116 colon cancer cell lines, which both have elevated levels of mTORC1 signaling. Both cell lines showed sensitivity to the treatment (Figures 3A and 3B). Combined treatment caused cell death at levels of 58.1% ± 18.5 in NCI-H460 cells and 55.1% ± 5.8 in HCT116 cells, significantly higher than with either agent alone. Both cell lines showed a higher level of caspase 8, caspase 3, and PARP cleavage following dual treatment when compared to single drug treatments (Figure 3C). Elevated levels of CHOP and GADD34 were observed in

nelfinavir and bortezomib treated cells, suggesting that cell death was likely mediated through the ER stress pathway.

### **2.3. Synergy of nelfinavir and bortezomib in inducing cell death in *Tsc2*<sup>-/-</sup> MEFs**

We next assessed evidence for synergy between nelfinavir and bortezomib in inducing cell death. *Tsc2*<sup>+/+</sup> and *Tsc2*<sup>-/-</sup> MEFs were treated with nelfinavir and bortezomib at a range of concentrations, both separately and in combination. Cells were then analysed by flow cytometry using DRAQ7 labelling (Figures 4A-D) revealing that nelfinavir has little cytotoxic effect as a single agent, especially at low doses (Figure 4A), whilst bortezomib potently induces cell death, more so in *Tsc2*<sup>-/-</sup> than *Tsc2*<sup>+/+</sup> cells (Figure 4B). Whilst *Tsc2*<sup>+/+</sup> MEFs can tolerate high concentrations of nelfinavir and bortezomib in combination (Figure 4C), *Tsc2*<sup>-/-</sup> MEFs are acutely sensitive to lower drug concentrations (Figure 4D). CompuSyn software was used to calculate combination index (CI) values based on mean cell death, which are shown as Chou-Talalay plots for *Tsc2*<sup>+/+</sup> (Figure 4E) and *Tsc2*<sup>-/-</sup> (Figure 4F) MEFs. Values below CI = 1 indicate synergy between nelfinavir with bortezomib. Figure 4F shows that nelfinavir and bortezomib act synergistically to induce cell death in *Tsc2*<sup>-/-</sup> MEFs at all concentrations used in this experiment.

### **2.4. Combined nelfinavir and bortezomib inhibit tumor spheroid formation and outgrowth of *Tsc2*<sup>-/-</sup> cells**

Based on the concentrations of nelfinavir and bortezomib that demonstrated synergy in *Tsc2*<sup>-/-</sup> MEFs, we utilised 20 nM bortezomib with 20  $\mu$ M nelfinavir in tumor formation assays. Nelfinavir alone did not impact colony formation and growth, but bortezomib treatment impaired growth by  $36 \pm 12\%$  (Figure 5A). When bortezomib was combined with nelfinavir, tumor growth was completely inhibited. To investigate whether nelfinavir and bortezomib could kill already established tumors, *Tsc2*<sup>-/-</sup> MEFs were cultured as spheroids using 3D cell culture before being treated over 96 h. Nelfinavir and bortezomib as single drug treatments and also in combination were compared to the mTORC1 inhibitor, rapamycin. Due to the prolonged treatment time compared to the 2D experiments, we utilised lower concentrations of nelfinavir (10  $\mu$ M) and bortezomib (10 nM) in this experiment. Cell death was measured by DRAQ7 staining intensity (Figure 5B) and compared to spheroid size (Figure 5C). Combined nelfinavir and bortezomib treatment caused a significant increase in DRAQ7 staining compared to both the single drug treatments and also when compared to rapamycin. However, rapamycin visibly shrank the overall size of the spheroid whereas treatments with either nelfinavir or bortezomib did not. To further determine viability, the treated spheroids shown in Figure 5B were plated into 2D cell culture systems and allowed to regrow without the presence of drug. Spheroid outgrowth was then measured over 72 h (Figure 5D, graphed in 5E). Spheroids treated with rapamycin, although shrunken, still contained viable cells that could rapidly grow out into culture. Spheroids treated with either nelfinavir or bortezomib also grew back, while there was no evidence of outgrowth in the combined treatment with nelfinavir and bortezomib. The lack

of cell recovery and the high level of DRAQ7 staining indicate that combined treatment with nelfinavir and bortezomib effectively prevents re-growth of spheroids through induction of cell death, whereas rapamycin shrank spheroids which then regrew when treatment was withdrawn, as previously reported in clinical studies with rapalogues [18,19]. The effect of nelfinavir and bortezomib in *Tsc2*<sup>-/-</sup> MEFs was validated in ELT3-V3 cells that showed a similar response (Supplementary Figure S2A-C). To further investigate how drug treatments affected tumor size and integrity, phalloidin (green) was used to stain the actin cytoskeleton, and DRAQ7 (far red) to counterstain nuclei, following drug treatment of *Tsc2*<sup>-/-</sup> MEFs. Figure 5F shows that rapamycin-treated spheroids retain a similar degree of actin fluorescence as DMSO-treated controls, whereas nelfinavir and bortezomib-treated spheroids exhibit comparatively less actin and nuclear staining. The weak nuclear staining and the collapse of the nuclear envelope is indicative of DNA fragmentation and suggests that nelfinavir-bortezomib is killing cells in the spheroid rather than causing senescence. This data supports our findings showing that rapamycin can shrink tumors, but without cytotoxic effects, while nelfinavir-bortezomib treatment is effective at causing cell death.

## ***2.5. Nelfinavir and bortezomib treatment downregulates pro-survival and upregulates pro-apoptosis genes, likely mediated through ER stress***

To gain a better understanding of the early changes that nelfinavir and bortezomib cause to gene expression within cells, RNA sequencing was performed in *Tsc2*<sup>+/+</sup> and *Tsc2*<sup>-/-</sup> MEFs after 6 h of combined treatment or DMSO vehicle control. Figure 6A shows a panel of genes associated with ER stress, a selection of which is highlighted graphically in Figure 6B (raw data in Supplementary Table 1). *Tsc2*<sup>-/-</sup> MEFs expressed higher basal levels of all the ER stress genes shown in the panel (Figure 6A, Supplementary Figure S3A and Supplementary Table 2). Following nelfinavir and bortezomib treatment, this expression was further increased (Supplementary Figure S3B and Supplementary Table 3), with expression in *Tsc2*<sup>-/-</sup> cells mostly significantly higher than that of the *Tsc2*<sup>+/+</sup> MEFs (Figure 6B). Figure 6C describes the changes of a panel of pro-survival and pro-death genes in *Tsc2*<sup>+/+</sup> versus *Tsc2*<sup>-/-</sup> dual-treated MEFs (genes selected based on AmiGO “cell death”). Figure 6C shows expression of pro-survival genes to be decreased, and pro-death genes to be increased in drug treated *Tsc2*<sup>-/-</sup> cells compared to treated *Tsc2*<sup>+/+</sup> MEFs. The overall RNA sequencing data is shown visually in a volcano plot (Figure 6D and Supplementary Table 4), with the genes in Figure 6C highlighted. To validate that the *Tsc2*<sup>+/+</sup> MEFs could efficiently restore ER homeostasis, while the *Tsc2*<sup>-/-</sup> MEFs could not, we carried out a time course of nelfinavir-bortezomib treatment (Figure 6E). We observed a strong initial increase in ATF4 and CHOP protein in both cell lines at 6 h of treatment, which was downregulated by 16 h to a level that was not significantly different to untreated. However, after 24 h of treatment, the protein expression of ATF4 and CHOP was enhanced in the *Tsc2*<sup>-/-</sup> MEFs, suggesting an inability to efficiently restore ER homeostasis. In contrast, the protein levels of ATF4 and CHOP remained low in the *Tsc2*<sup>+/+</sup> MEFs after 24 h of treatment.

## **2.6. Nelfinavir and bortezomib treatment reduced tumor volume in ELT-V3 mouse xenografts, correlating with increased CHOP expression in tumor tissue**

To determine the anti-tumor efficacy of nelfinavir and bortezomib *in vivo*, mice bearing *Tsc2*-null ELT3 xenograft tumors were treated with the drugs as single agents or in combination. Thirty-five days after commencement of treatment, combined nelfinavir and bortezomib decreased tumor growth by approximately 70% which was a significant decrease compared with vehicle-treated mice (Figure 7A). The single agent treatments slowed tumor growth but not significantly. While combined treatment of nelfinavir and bortezomib is well tolerated in patients [11], combined treatment was not well tolerated in mice. In the combination group, 11/14 mice died or were euthanized due to excessive toxicity compared with 2/14 in the vehicle treated group, 5/14 in the nelfinavir alone group and 5/14 in the bortezomib alone group. Immunohistochemical analysis of xenograft tumor tissue sections revealed a modest increase in CHOP positive cells after nelfinavir and bortezomib combined treatment (Figure 7B). The heterogeneity of CHOP staining likely reflects cycles of ER stress induction and recovery in these cells. By western blot analysis, a higher level of ATF4 protein and PARP cleavage was observed in tumors from mice that were treated with both nelfinavir and bortezomib (Figure 7C), which indicates an elevated level of ER stress and cell death upon combined drug treatment.

## **3. Discussion**

In this study, using clinically relevant drugs that could be repositioned to treat tumors displaying high ER stress profiles, we reveal that mTORC1-overactive cells are sensitive to combined nelfinavir and bortezomib treatment. We show that nelfinavir and bortezomib act to amplify ER stress levels, and combine synergistically to promote cell death. Whilst wild-type cells tolerate this drug combination with minimal cell death, cytotoxicity in *Tsc2*-deficient cells is evident even at low drug concentrations and is likely attributable to their inability to manage the ER stress burden. Indeed, we see that ER stress is not fully restored in the *Tsc2*-deficient cells after 24 h of combined drug treatment, as observed by a reoccurrence of ATF4 and CHOP protein expression (Figure 6E). It was previously reported that *Tsc2*-deficient cells have a truncated ER stress response [20], which fits with our observation that cells lacking functional *Tsc2* are compromised in their ability to reduce their ER stress burden and restore ER homeostasis. *Tsc2* functions as an important component of the survival arm during ER stress as it is positioned downstream of several ER stress-mediated survival pathways. One pathway involves GADD34, which associates with *Tsc2* to recruit protein phosphatase 1 (PP1) to dephosphorylate and activate *Tsc2*, thus repressing mTORC1 signal transduction. We observed high protein expression levels of GADD34 after ER stress induction in all our cell lines, more so in *Tsc2*<sup>-/-</sup> MEFs.

Normally, protein synthesis is down-regulated upon ER stress as an efficient strategy to prevent further build-up of unfolded protein within the ER. We observed that *Tsc2*-deficient cells have elevated protein synthesis despite the higher background levels of ER stress, with

a 3 to 4-fold increase in protein synthesis in *Tsc2*<sup>-/-</sup> MEFs compared to wild-type (Figure 1F). The elevated levels of protein synthesis would likely enhance ER stress within the *Tsc2*-deficient cells. As well as promoting translation, mTORC1 hyperactivation increases the activity of the proteasome while reducing autophagy [6]. Downregulation of autophagy means the proteasome becomes the principal mechanism to reduce ER stress via protein degradation in mTORC1-driven cells. However, the proteasome inhibitor, bortezomib, had a lack of *in vivo* activity against renal tumors in *Tsc2*<sup>+/-</sup> mice as a single agent [9], perhaps reflecting a failure to induce a sufficient level of ER stress. This problem could potentially be overcome by using a combination of two ER stress inducing agents, such as nelfinavir and bortezomib.

Bortezomib (Velcade, Janssen-Cilag) was the first FDA-approved proteasome inhibitor found to have clinical promise for treating cancer. Bortezomib was originally approved for the treatment of advanced multiple myeloma and more recently for mantle cell lymphoma. Next generation proteasome inhibitors (marizomib and carfilzomib) are currently being tested in clinical trials. Bortezomib's action is to specifically bind to the catalytic site of the 26S proteasome to inhibit enzyme activity. As a consequence of inhibiting the ubiquitin-proteasome system, bortezomib markedly changes the survival status of cancer cells. The synergy observed between nelfinavir and bortezomib is unlikely due to ER stress alone, but probably involves other processes impacted by treatment. Additional processes affected upon proteasome inhibition include cell cycle control, apoptosis, angiogenesis, transcriptional regulation and DNA-damage response (see review [21]). Although the nelfinavir and bortezomib combination showed considerable toxicity in mice in our study, a recent phase I clinical trial (clinicaltrials.gov: NCT01164709) in bortezomib-refractory multiple myeloma combining bortezomib with nelfinavir was well tolerated, safe and showed promising activity [11]. Supporting this, treatment of patients with a recommended dose for a phase II trial of advanced haematological malignancies showed that 9 relapse patients whose malignancies were resistant to bortezomib had either a partial response or clinical benefit when bortezomib was combined with nelfinavir, with no apparent increase in toxicity [11].

Our work demonstrates for the first time that functional loss of TSC2 and subsequent mTORC1 hyperactivation sensitises cells to combined proteasomal inhibition and ER stress induction. Our findings have clinical relevance in stratified medicine, where cancers with compromised signal transduction through TSC1/2-mTORC1 (via upstream pathways e.g. oncogenic K-RAS or loss of PTEN) may be sensitive to nelfinavir and bortezomib. Our data implies that a high ER stress burden and hyperactive mTORC1 signaling could function as predictive biomarkers of drug efficacy when considering combined nelfinavir and bortezomib treatment.

364

## 365 **4. Materials and Methods**

### 366 **4.1. Cell culture and reagents**

367 *Tsc2*<sup>+/+</sup> *p53*<sup>-/-</sup> and *Tsc2*<sup>-/-</sup> *p53*<sup>-/-</sup> mouse embryonic fibroblasts (MEFs) were a kind gift from  
368 David Kwiatkowski (Harvard University, Boston, USA) in 2004 and have been previously  
369 characterised [22]. Eker rat leiomyoma-derived *Tsc2*-deficient ELT3-V3 cells and matching  
370 control *TSC2*-expressing ELT3-T3 cells generated in Astrinidis et al, 2002 [23], were kindly  
371 provided in 2006 by Cheryl Walker (M.D. Anderson Cancer Center, Houston, USA). Human  
372 lung carcinoma (NCI-H460) cells were purchased from ATCC in 2012 while HCT116 cells were  
373 provided in 2015 by Nick Leslie (Heriot Watt University, Edinburgh). All cell lines were  
374 mycoplasma free and regularly tested for mycoplasma infection using the Venor GeM  
375 Classic PCR kit from Cambio. All cell lines were cultured in Dulbecco's Modified Eagle's  
376 Medium (DMEM, Lonza, Basel, Switzerland, BE12-604F), supplemented with 10 % (v/v)  
377 foetal bovine serum (FBS, 10270106, Thermo Fisher Scientific), 100 U/ml penicillin and 100  
378 µg/ml streptomycin (P4333, Sigma-Aldrich, Dorset, UK) in a humidified incubator at 37 °C, 5  
379 % (v/v) CO<sub>2</sub>. Nelfinavir mesylate hydrate (PZ0013), thapsigargin (T9033), MG132 (C2211)  
380 and etoposide (E1383) were purchased from Sigma, while bortezomib (CAS 179324-69-7),  
381 rapamycin (CAS 53123-88-9), Z-VAD-FMK (CAS 161401-82-7), and GSK2606414 were  
382 purchased from Merck Millipore (Hertfordshire, UK).

### 383 **4.2. mRNA extraction, reverse transcription, XBP1 splicing, Chop and Bip qPCR**

384 Samples were collected and analysed as previously described [15]. *Bip* was analysed using  
385 Quantitect primers (QT00172361, Qiagen).

### 386 **4.3. Western Blotting**

387 Both live and dead cells were collected and lysed in radio immunoprecipitation assay (RIPA)  
388 buffer (R0278) supplemented with Complete Mini protease inhibitor cocktail  
389 (11836170001), PhosSTOP phosphatase inhibitor cocktail (04906837001) and 1 mM  
390 dithiothreitol (DTT, D0632) (all purchased from Sigma). Following sonication, equal amounts  
391 of protein were loaded and western blotting was performed as previously described [24].  
392 Protein from xenograft tumors were extracted by AllPrep DNA/RNA/Protein Mini Kit using  
393 the manufacturers protocol (Qiagen). Antibodies towards C/EBP homologous protein  
394 (CHOP, #2895), inositol-requiring and ER-to-nucleus signaling protein 1α (IRE1α, #3294S),  
395 ATF4 (#11815), caspase-3 (#9662), caspase-8 (mouse specific #4927, human specific #9746),  
396 PARP (#9542), TSC2 (#3990) and β-actin (#4967) were purchased from Cell Signaling  
397 Technology (Danvers, USA). Growth arrest and DNA damage-inducible protein 34 (GADD34,  
398 also known as Protein phosphatase 1 regulatory subunit 15A [PPP1R15A], 10449-1-AP)  
399 antibody was purchased from Proteintech (Manchester, UK). Ubiquitin antibody was from  
400 BioMol (PW8810). Densitometry was carried out using ImageJ (version 1.51j8).

401

#### 402 **4.4. Late cell death assay and determination of drug synergy**

403 Cell death was quantified as previously described [15]. To determine synergy, cells were  
404 treated with a range of drug concentrations and the affected fraction was used to  
405 determine combination index (CI) values using CompuSyn software (ComboSyn, Inc.) using a  
406 non-constant ratio approach.

#### 407 **4.5. DNA fragmentation ELISA**

408 DNA fragmentation was measured with the Cell Death Detection ELISA kit (Roche) according  
409 to the manufacturer's protocol. This is a one-step colorimetric sandwich ELISA that  
410 quantifies DNA fragments. *Tsc2*<sup>+/+</sup> and *Tsc2*<sup>-/-</sup> MEFs were plated in 96-well plates and  
411 incubated overnight. Drugs were added to the cells and incubated for 24 h and DNA  
412 fragmentation assayed. The relative quantity of immobilized antibody histone complex was  
413 determined photometrically (at 405 nm) using 2,2,0-azino-bis-3-ethylbenzothiazoline-6-  
414 sulfonic acid as a peroxidase substrate.

#### 415 **4.6 Proteasome Activity Analysis**

416 Proteasomes were extracted from live cells 2 h post-treatment and their chymotrypsin-like  
417 proteasome activity determined according to a previously described protocol [25].

#### 418 **4.7 Soft Agar Assay, spheroids and outgrowth**

419 Soft agar assays, spheroid formation and outgrowth analysis was performed as previously  
420 described [26]. For phalloidin staining, spheroids were grown over 96 h and drug treated for  
421 72 h, before fixing in 4% paraformaldehyde for 30 min. Spheroids were permeabilized using  
422 0.1% Triton-X100 for 45 min before staining with ActinGreen 488 Ready Probes Reagent  
423 (R37110, Thermo Fisher) as per manufacturers protocol. Finally, spheroids were stained  
424 with 3  $\mu$ M DRAQ7 (DR71000, Biostatus) before transfer to a glass-bottomed plate and  
425 imaged using a Zeiss LSM 880 confocal microscope with Zen software. Analysis was  
426 performed using ImageJ v1.50i.

#### 427 **4.8 RNA-Seq sample preparation, sequencing and analysis**

428 Total RNA quality and quantity was assessed using Agilent 2100 Bioanalyser and a RNA Nano  
429 6000 kit (Agilent Technologies). 100-900 ng of total RNA with a RIN value >8 was depleted of  
430 ribosomal RNA and the sequencing libraries were prepared using the Illumina® TruSeq®  
431 Stranded total RNA with Ribo-Zero Gold™ kit (Illumina Inc.). The steps included rRNA  
432 depletion and cleanup, RNA fragmentation, 1st strand cDNA synthesis, 2nd strand cDNA  
433 synthesis, adenylation of 3' ends, adapter ligation, PCR amplification (12-cycles) and  
434 validation. The manufacturer's instructions were followed except for the cleanup after the  
435 ribozero depletion step where Ampure®XP beads (Beckman Coulter) and 80% Ethanol were



used. The libraries were validated using the Agilent 2100 Bioanalyser and a high-sensitivity kit (Agilent Technologies) to ascertain the insert size, and the Qubit® (Life Technologies) was used for quantitation. Following validation, the libraries were normalized to 4 nM, pooled together and clustered on the cBot™ 2 following the manufacturer's recommendations. The pool was then sequenced using a 75-base paired-end (2x75bp PE) dual index read format on the Illumina® HiSeq2500 in high-output mode according to the manufacturer's instructions. Quality control checks of the resultant reads were performed using FastQC before mapping to the UCSC mouse mm10 reference genome using Tophat and Bowtie. Differentially expressed transcripts were identified using a DeSeq2 analysis [27] on normalised count data with the design formula setup to analyse all pairwise comparisons in the dataset using contrasts. The resultant p-values were corrected for multiple testing and false discovery issues using the FDR method. Genes involved in cell survival were selected based on GO:0008219 (cell death) from the complete list on AmiGo 2 (<http://amigo.geneontology.org/amigo/landing>).

#### **4.9 Protein translation assay**

This was performed as in [28], using EasyTag™ EXPRESS-[<sup>35</sup>S] Protein Labeling Mix (NEG772007MC, Perkin Elmer).

#### **4.10 ELT-3 mouse xenograft**

All animal experimental procedures were approved by the Institutional Animal Care and Use Committee of CrownBIO prior to conduct. During the study, the care and use of animals was conducted in accordance with the regulations of the Association for Assessment and Accreditation of Laboratory Animal Care (AAALAC). A mouse xenograft model was established using ELT3-V3 cells inoculated into 9-10 week old female NOD/SCID mice (HFK Bio-Technology Co. Ltd. (Beijing, China)). Sample size was based upon using a two tailed t-test, assuming unequal variance and large effect size of 0.8 with 60 % power at the 10 % significance level. Exponentially growing ELT3-V3 cells were used for tumor inoculation. One week prior to cell inoculation, all the mice were implanted with 17-β estradiol pellets (2.5 mg, 90-day release, Innovative Research of America). Mice were inoculated subcutaneously at the right flank with ELT3-V3 cells ( $5 \times 10^6$ ) in 0.2 ml of PBS. Tumor volumes were measured in two dimensions using a calliper, and the volume was expressed in mm<sup>3</sup> using the formula:  $V = 0.5 a \times b^2$  where a and b are the long and short diameters of the tumor, respectively. Grouping and treatments began when the mean tumor size reached 186 mm<sup>3</sup>. Fourteen mice were assigned per treatment group using a randomized block design, based on their tumor volumes to receive one of the following treatments: 1) vehicle (4 % (v/v) DMSO, 5 % (v/v) PEG, 5 % (v/v) TWEEN 80 in saline); 2) nelfinavir, 50 mg/kg dissolved in vehicle; 3) bortezomib, 0.5 mg/kg dissolved in 0.04 % (v/v) mannitol solution; 4) nelfinavir, 50 mg/kg and bortezomib, 0.5 mg/kg. Treatments were administered intraperitoneally on days 1, 3, 5, 8, 10, 12, 15 and 17. Dosages were reduced to 30 mg/kg nelfinavir and 0.3 mg/kg bortezomib on day 8 due to toxicity. Tumor volumes were measured three times per week.

Investigators were not blinded to the group allocation. Due to lower numbers of mice than anticipated at Day 17, groups were compared non-parametrically using the Kruskal-Wallis test and pairwise comparisons.

**4.11 Immunohistochemistry**

Tumors were snap frozen in optimal cutting temperature compound and cryostat sectioned at 10 µm thickness. Sections were warmed to room temperature for 30 min, fixed in ice cold acetone for 5 min and air-dried for 30 min. Following blocking in 5% (v/v) normal goat serum (NGS) in Tris Buffered Saline (pH 7.6) 0.1 % (v/v) Tween-20, sections were incubated over-night at 4°C with 1/1000 rabbit monoclonal antibody against CHOP(Abcam, ab179823), blocked with Envision peroxidase block and incubated for 30 min in Envision rabbit polymer, before detection with DAB chromogen (all DAKO). Slides were counterstained with haematoxylin, dehydrated through an ethanol series and xylene, before mounting in DPX medium (Fisher Scientific). 5 fields from each tumor were scored for percentage of cells staining positively for CHOP (ImageJ, v1.51j8).

**4.12 Statistical analysis**

At least three independent, biological repeats were performed for each experiment. Exact sample size is indicated in each figure legend. Results are expressed as mean ± standard deviation (SD), unless otherwise specified in the figure legend. Data analysis was carried out using a one-way ANOVA followed by LSD post-hoc test, or an independent samples Kruskal-Wallis test as appropriate. Significance is reported at \* p < 0.05, \*\* p < 0.01, \*\*\* p < 0.001, and NS = not significant.

**Conflict of Interest Statement**

RJE is non-executive director of Biostatus Ltd, the vendor of DRAQ7.

**Acknowledgements**

This work was supported by Health and Care Research Wales (the Wales Cancer Research Centre) (to ED, AT, PG and TH), the Tuberous Sclerosis Association (to ED, AT and MS), Cancer Research Wales (to CJ, RJE and AT), the Tuberous Sclerosis Alliance (to ED and AT), the Hospital Saturday Fund (to AT) and BBSRC (to RJE). We would like to thank the Wales Gene Park for their contribution to this study.

**References**

1. Clarke HJ, Chambers JE, Liniker E, Marciniak SJ. Endoplasmic reticulum stress in malignancy. *Cancer Cell* 2014; **25**: 563–573.

- 511 2. Appenzeller-Herzog C, Hall MN. Bidirectional crosstalk between endoplasmic reticulum  
512 stress and mTOR signaling. *Trends Cell Biol* 2012; **22**: 274–282.
- 513 3. Dunlop EA, Tee AR. mTOR and autophagy: a dynamic relationship governed by nutrients  
514 and energy. *Semin Cell Dev Biol* 2014; **36**: 121–129.
- 515 4. Stengel S, Messner B, Falk-Paulsen M, Sommer N, Rosenstiel P. Regulated proteolysis as  
516 an element of ER stress and autophagy: Implications for intestinal inflammation. *Biochim*  
517 *Biophys Acta* 2017; **1864**: 2183–2190.
- 518 5. Lam HC, Nijmeh J, Henske EP. New developments in the genetics and pathogenesis of  
519 tumours in tuberous sclerosis complex. *J Pathol* 2017; **241**: 219–225.
- 520 6. Zhang Y, Nicholatos J, Dreier JR, Ricoult SJ, Widenmaier SB, Hotamisligil GS, *et al.*  
521 Coordinated regulation of protein synthesis and degradation by mTORC1. *Nature* 2014; **513**:  
522 440–3.
- 523 7. Siroky BJ, Yin H, Babcock JT, Lu L, Hellmann AR, Dixon BP, *et al.* Human TSC-associated  
524 renal angiomyolipoma cells are hypersensitive to ER stress. *Am J Physiol Renal Physiol* 2012;  
525 **303**: F831–844.
- 526 8. Babcock JT, Nguyen HB, He Y, Hendricks JW, Wek RC, Quilliam LA. Mammalian target of  
527 rapamycin complex 1 (mTORC1) enhances bortezomib-induced death in tuberous sclerosis  
528 complex (TSC)-null cells by a c-MYC-dependent induction of the unfolded protein response. *J*  
529 *Biol Chem* 2013; **288**: 15687–15698.

- 530 9. Auricchio N, Malinowska I, Shaw R, Manning BD, Kwiatkowski DJ. Therapeutic trial of  
531 metformin and bortezomib in a mouse model of tuberous sclerosis complex (TSC). *PLoS One*  
532 2012; **7**: e31900.
- 533 10. Gills JJ, Lopiccolo J, Tsurutani J, Shoemaker RH, Best CJ, Abu-Asab MS, *et al.* Nelfinavir, A  
534 lead HIV protease inhibitor, is a broad-spectrum, anticancer agent that induces endoplasmic  
535 reticulum stress, autophagy, and apoptosis in vitro and in vivo. *Clin Cancer Res* 2007; **13**:  
536 5183–5194.
- 537 11. Driessen C, Kraus M, Joerger M, Rosing H, Bader J, Hitz F, *et al.* Treatment with the HIV  
538 protease inhibitor nelfinavir triggers the unfolded protein response and may overcome  
539 proteasome inhibitor resistance of multiple myeloma in combination with bortezomib: a  
540 phase I trial (SAKK 65/08). *Haematologica* 2016; **101**: 346–355.
- 541 12. Shim JS, Rao R, Beebe K, Neckers L, Han I, Nahta R, *et al.* Selective inhibition of HER2-  
542 positive breast cancer cells by the HIV protease inhibitor nelfinavir. *J Natl Cancer Inst* 2012;  
543 **104**: 1576–1590.
- 544 13. Kraus M, Müller-Ide H, Rückrich T, Bader J, Overkleeft H, Driessen C. Ritonavir, nelfinavir,  
545 saquinavir and lopinavir induce proteotoxic stress in acute myeloid leukemia cells and  
546 sensitize them for proteasome inhibitor treatment at low micromolar drug concentrations.  
547 *Leuk Res* 2014; **38**: 383–392.
- 548 14. Kawabata S, Gills JJ, Mercado-Matos JR, Lopiccolo J, Wilson W 3rd, Hollander MC, *et al.*  
549 Synergistic effects of nelfinavir and bortezomib on proteotoxic death of NSCLC and multiple  
550 myeloma cells. *Cell Death Dis* 2012; **3**: e353.

- 551 15. Johnson CE, Hunt DK, Wiltshire M, Herbert TP, Sampson JR, Errington RJ, *et al.*  
552 Endoplasmic reticulum stress and cell death in mTORC1-overactive cells is induced by  
553 nelfinavir and enhanced by chloroquine. *Mol Oncol* 2015; **9**: 675–688.
- 554 16. Kraus M, Bader J, Overkleeft H, Driessen C. Nelfinavir augments proteasome inhibition  
555 by bortezomib in myeloma cells and overcomes bortezomib and carfilzomib resistance.  
556 *Blood Cancer J* 2013; **3**: e103.
- 557 17. Astrinidis A, Cash TP, Hunter DS, Walker CL, Chernoff J, Henske EP. Tuberin, the tuberous  
558 sclerosis complex 2 tumor suppressor gene product, regulates Rho activation, cell adhesion  
559 and migration. *Oncogene* 2002; **21**: 8470–8476.
- 560 18. Peng ZF, Yang L, Wang TT, Han P, Liu ZH, Wei Q. Efficacy and safety of sirolimus for renal  
561 angiomyolipoma in patients with tuberous sclerosis complex or sporadic  
562 lymphangiomyomatosis: a systematic review. *J Urol* 2014; **192**: 1424–1430.
- 563 19. Dabora SL, Franz DN, Ashwal S, Sagalowsky A, DiMario FJ Jr, Miles D, *et al.* Multicenter  
564 phase 2 trial of sirolimus for tuberous sclerosis: kidney angiomyolipomas and other tumors  
565 regress and VEGF- D levels decrease. *PLoS One* 2011; **6**: e23379.
- 566 20. Kang YJ, Lu MK, Guan KL. The TSC1 and TSC2 tumor suppressors are required for proper  
567 ER stress response and protect cells from ER stress-induced apoptosis. *Cell Death Differ*  
568 2011; **18**: 133–144.
- 569 21. Gandolfi S, Laubach JP, Hideshima T, Chauhan D, Anderson KC, Richardson PG. The  
570 proteasome and proteasome inhibitors in multiple myeloma. *Cancer Metastasis Rev* 2017;  
571 **36**: 561–584.

22. Zhang H, Cicchetti G, Onda H, Koon HB, Asrican K, Bajraszewski N, Vazquez F, Carpenter CL, Kwiatkowski DJ. Loss of Tsc1/Tsc2 activates mTOR and disrupts PI3K-Akt signaling through downregulation of PDGFR. *J. Clin. Invest.* 2003; 112: 1223-1233.
23. Astrinidis A, Cash TP, Hunter DS, Walker CL, Chernoff J, Henske EP. Tuberin, the tuberous sclerosis complex 2 tumor suppressor gene product, regulates Rho activation, cell adhesion and migration. *Oncogene*. 2002; 21: 8470-8476.
24. Dunlop EA, Hunt DK, Acosta-Jaquez HA, Fingar DC, Tee AR. ULK1 inhibits mTORC1 signaling, promotes multisite Raptor phosphorylation and hinders substrate binding. *Autophagy* 2011; 7: 737-747.
25. Crawford LJ, Walker B, Ova H, Chauhan D, Anderson KC, Morris TC, *et al.* Comparative selectivity and specificity of the proteasome inhibitors BzLLCOCHO, PS-341, and MG-132. *Cancer Res* 2006; 66: 6379–6386.
26. Dunlop EA, Johnson CE, Wiltshire M, Errington RJ, Tee AR. Targeting protein homeostasis with nelfinavir/salinomycin dual therapy effectively induces death of mTORC1 hyperactive cells. *Oncotarget* 2017; 8: 48711–48724.
27. Love MI, Huber W, Anders S. Moderated estimation of fold change and dispersion for RNA-seq data with DESeq2. *Genome Biol* 2014; 15: 550.
28. Tee AR, Proud CG. DNA-damaging agents cause inactivation of translational regulators linked to mTOR signalling. *Oncogene* 2000; 19: 3021–3031.

## Figure Legends

**Figure 1 – Nelfinavir markedly enhances ER stress in *Tsc2*<sup>-/-</sup> MEFs when combined with proteasome inhibitors.** (A) *Tsc2*<sup>+/+</sup> and *Tsc2*<sup>-/-</sup> MEFs were treated for 6 h with either DMSO vehicle, 20  $\mu$ M nelfinavir (NFV), 1  $\mu$ M MG132, 50 nM bortezomib (BTZ), alone or in combination where indicated. Cells were harvested and total protein levels of TSC2, IRE1 $\alpha$ , ATF4, CHOP, GADD34 and  $\beta$ -actin were detected by western blot. Anti-ubiquitin antibodies were used to determine the relative level of poly-ubiquitinated protein (n=3). (B) *Xbp1* mRNA splicing was determined following treatments as indicated. PCR products were resolved on agarose gels (unspliced = 480 bp upper band, spliced = 454 bp lower band, n=3). The proportion of spliced *Xbp1* (*Xbp1s*) is graphed below. (C) *Chop* and *Bip* mRNA levels were analysed following 6 h dual treatment and standardised against *Actb* mRNA (n=3). (D) *Tsc2*<sup>-/-</sup> MEFs were pre-treated with 2  $\mu$ M GSK2606414 (PERK inhibitor) for 30 min, where indicated, before being treated with 20  $\mu$ M nelfinavir and 50 nM bortezomib for 6 h. Protein expression for CHOP and  $\beta$ -actin was then determined by western blot analysis (n=3). (E) The proteasome activity of drug-treated samples, as indicated, was determined by monitoring the turnover of the fluorescent chymotrypsin-like substrate (n=3). Statistics given are relative to the *Tsc2*<sup>+/+</sup> DMSO control. (F) Levels of protein synthesis were determined for control, single and dual treated cells as indicated (n=5).

**Figure 2 – Nelfinavir enhances the cytotoxicity of bortezomib in *Tsc2*<sup>-/-</sup> but not in *Tsc2*<sup>+/+</sup> MEFs.** (A) *Tsc2*<sup>+/+</sup> and *Tsc2*<sup>-/-</sup> MEFs were treated with either DMSO vehicle, 1  $\mu$ M MG132, 50 nM bortezomib (BTZ), 20  $\mu$ M nelfinavir (NFV) alone or in combination where indicated over 24 h. Cells were then subjected to flow cytometry following DRAQ7 staining. DRAQ7 exclusion (below line) represents the viable cell population, whilst positive DRAQ7 staining (above line) indicates cell death. The number of DRAQ7-stained *Tsc2*<sup>+/+</sup> and *Tsc2*<sup>-/-</sup> MEFs are graphed in (B) (n=3). (C) *Tsc2*<sup>+/+</sup> and *Tsc2*<sup>-/-</sup> MEFs were treated for 24 h with either DMSO, 20  $\mu$ M nelfinavir (NFV), 50 nM bortezomib (BTZ) as single agents or in combination, as indicated, and then subjected to DNA fragmentation assays (n=5). (D) *Tsc2*<sup>+/+</sup> and *Tsc2*<sup>-/-</sup> MEFs were treated for 24 h with 20  $\mu$ M NFV combined with 50 nM BTZ in the presence or absence of 20  $\mu$ M Z-VAD-FMK and analysed for cell death by flow cytometry with DRAQ7 staining. The number of DRAQ7-stained *Tsc2*<sup>+/+</sup> and *Tsc2*<sup>-/-</sup> MEFs are graphed (n=3).

**Figure 3 – Nelfinavir enhances the cytotoxicity of bortezomib in human lung and colon cancer cell lines.** (A) NCI-H460 lung cancer and HCT116 colon cancer cells were treated with either DMSO vehicle, 50 nM bortezomib (BTZ), 20  $\mu$ M nelfinavir (NFV) alone, or NFV combined with BTZ over 24 h. Cells were then subjected to flow cytometry with DRAQ7 staining. DRAQ7 exclusion (below line) represents the viable cell population, whilst positive DRAQ7 staining (above line) indicates cell death. The number of DRAQ7-stained cells are graphed in (B) (n=3). (C) With the addition of Etoposide (100  $\mu$ M), cells were treated as in (A) and total protein levels of Caspase-8 (CASP8), Caspase-3 (CASP3), PARP, GADD34, CHOP and  $\beta$ -actin were measured by western blot analysis (n=3).

**Figure 4 – Nelfinavir and bortezomib synergise to selectively kill *Tsc2*<sup>-/-</sup> MEFs.** Dose response curves were performed in *Tsc2*<sup>+/+</sup> and *Tsc2*<sup>-/-</sup> MEFs using flow cytometry as a readout of cell death for nelfinavir (A), bortezomib (B) and the combination (C, D) (n=3). Synergy was assessed by examining cell death across a range of bortezomib concentrations, with or without 20  $\mu$ M nelfinavir and calculated using CompuSyn software (E, F). Graphs show mean  $\pm$  S.E.M.

**Figure 5 – Nelfinavir and bortezomib prevent tumor spheroid growth in *Tsc2*<sup>-/-</sup> MEFs.** (A) *Tsc2*<sup>-/-</sup> MEFs were plated in soft agar and treated over 11 days with either 20  $\mu$ M nelfinavir (NFV), 20 nM bortezomib (BTZ), as single agents or in combination. Images of the colonies were taken and the diameters measured using ImageJ. Scale bar is 20  $\mu$ m (n=4, with >100 spheroids measured per condition, per replicate). (B) *Tsc2*<sup>-/-</sup> MEF spheroids were treated with DMSO vehicle control, 10  $\mu$ M nelfinavir combined with 10 nM bortezomib (NFV BTZ), or 25 nM rapamycin (RAP), for 96 h. DRAQ7 was added for the final 36 h to monitor cell death before images were taken and quantified (n $\geq$ 3, average of 12 spheroids per condition per replicate). (C) Spheroid diameter was determined from phase contrast images of (B) after 96 h drug treatment and plotted against DRAQ7 staining intensity. (D) Spheroids were re-plated onto standard tissue culture plates and grown under drug-free conditions. Images were taken every 24 h and the area of outgrowth calculated using Image J. Scale bar is 200  $\mu$ m. Relative outgrowth areas are graphed in (E). Statistics compare the 72 h timepoint. Graphs in A, B and E shown mean  $\pm$  S.E.M. (F) Treated spheroids were stained using phalloidin (actin - green in merged images) and DRAQ7 (nuclei - white) and imaged using confocal microscopy. A representative slice (x63 oil lens) through the spheroid is shown with a scale bar of 30  $\mu$ m, alongside the maximum projection (x20 lens) with a scale bar of 75  $\mu$ m.

**Figure 6 – Nelfinavir and bortezomib upregulate early response genes for ER stress and cell death in *Tsc2*<sup>-/-</sup> MEFs, whilst pro-survival genes are downregulated.** *Tsc2*<sup>+/+</sup> and *Tsc2*<sup>-/-</sup> MEFs were treated with either DMSO vehicle or combined nelfinavir (20  $\mu$ M) and bortezomib (50 nM) for 6 h before processing for RNA sequencing (n=3). (A) Heatmap of a panel of ER stress-linked genes, a selection of which are highlighted graphically in (B). (C) Paired heatmaps from dual treated cells showing early response genes linked to cell survival and death which are highlighted in a volcano plot (D). (E) *Tsc2*<sup>+/+</sup> and *Tsc2*<sup>-/-</sup> MEFs were treated with either DMSO vehicle or combined nelfinavir (20  $\mu$ M) and bortezomib (50 nM) for 6 h, 16 h, and 24 h before extracting protein for western blot and probing for ATF4, CHOP, or  $\beta$ -actin (n=3).

**Figure 7 – Nelfinavir and bortezomib significantly reduce tumor volume in ELT3-V3 mouse xenografts, likely mediated through increased CHOP activity.** ELT3-V3 tumor xenografts (n=14 per group) were treated with either vehicle control, 5mg/ml nelfinavir (NFV), 0.05mg/ml bortezomib (BTZ), or NFV and BTZ in combination by intraperitoneal injection. (A) Tumor volume was recorded over 35 days before remaining mice were euthanised.



673 Significant reduction of tumor volume was observed at day 35 when comparing  
674 combination to vehicle control. (B) Representative images of tumors stained with  
675 haematoxylin (to indicate cell nuclei, blue) and an antibody against CHOP (brown). The  
676 percentage of CHOP-positive cells per treatment is indicated. (C) Western blot for ATF4,  
677 PARP cleavage, or  $\beta$ -actin were carried out in triplicate per treatment.

678 **Figure S1 - Nelfinavir enhances the cytotoxicity of bortezomib in ELT3-V3 but not in ELT3-**  
679 **T3 cells** (A) ELT3-V3 and ELT3-T3 cells were treated with either DMSO vehicle, 1  $\mu$ M MG132,  
680 50 nM bortezomib (BTZ), 20  $\mu$ M nelfinavir (NFV) alone, or NFV combined with either MG132  
681 or BTZ over 24 h. Cells were then subjected to flow cytometry with DRAQ7 staining. DRAQ7  
682 exclusion (below line) represents the viable cell population, whilst positive DRAQ7 staining  
683 (above line) indicates cell death. The number of DRAQ7-stained ELT3-V3 and ELT3-T3 cells  
684 are graphed in (B) (n=3). (C) Cells were treated as in (A) and total protein levels of Caspase-8  
685 (CASP8), Caspase-3 (CASP3), PARP, and  $\beta$ -actin were measured by western blot analysis.

686 **Figure S2 – Nelfinavir and bortezomib prevent tumor spheroid growth in ELT3-V3 cells.** (A)  
687 ELT3-V3 spheroids were treated with DMSO vehicle control, 10  $\mu$ M nelfinavir (NFV)  
688 combined with 10 nM bortezomib (BTZ), or 25 nM rapamycin (RAP), for 96 h. DRAQ7 was  
689 added for the final 36 h to monitor cell death before images were taken and quantified. (B)  
690 Spheroid diameter was determined from phase contrast images of (A) after 96 h drug  
691 treatment and plotted against DRAQ7 staining intensity. (C) Spheroids were then re-plated  
692 onto standard tissue culture plates and grown under drug-free conditions. Images were  
693 taken every 24 h and the area of outgrowth calculated using Image J.

694 **Figure S3 – *Tsc2*<sup>-/-</sup> MEFs have an increased basal level of ER stress which is exacerbated by**  
695 **nelfinavir and bortezomib treatment.** (A) RNA sequencing data from DMSO vehicle-treated  
696 *Tsc2*<sup>+/+</sup> and *-/-* MEFs was compared for basal gene expression changes. Genes linked to the  
697 ER stress response are highlighted. (B) RNA sequencing data from DMSO vehicle-treated  
698 *Tsc2*<sup>-/-</sup> MEFs and those treated with nelfinavir and bortezomib was compared for gene  
699 expression changes. Genes linked to the ER stress response are highlighted (n=3).

**Figure 1**

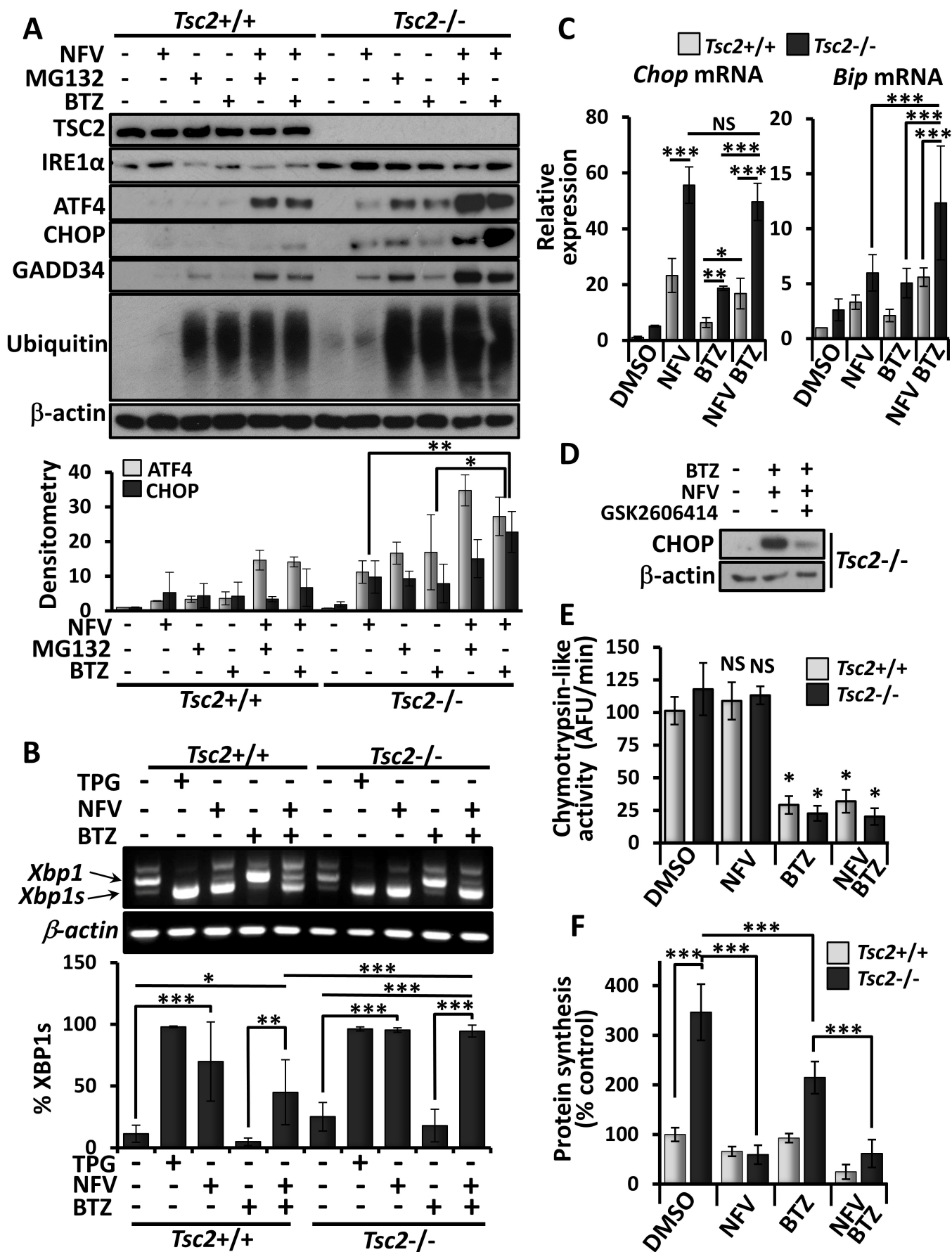


**Figure 2**

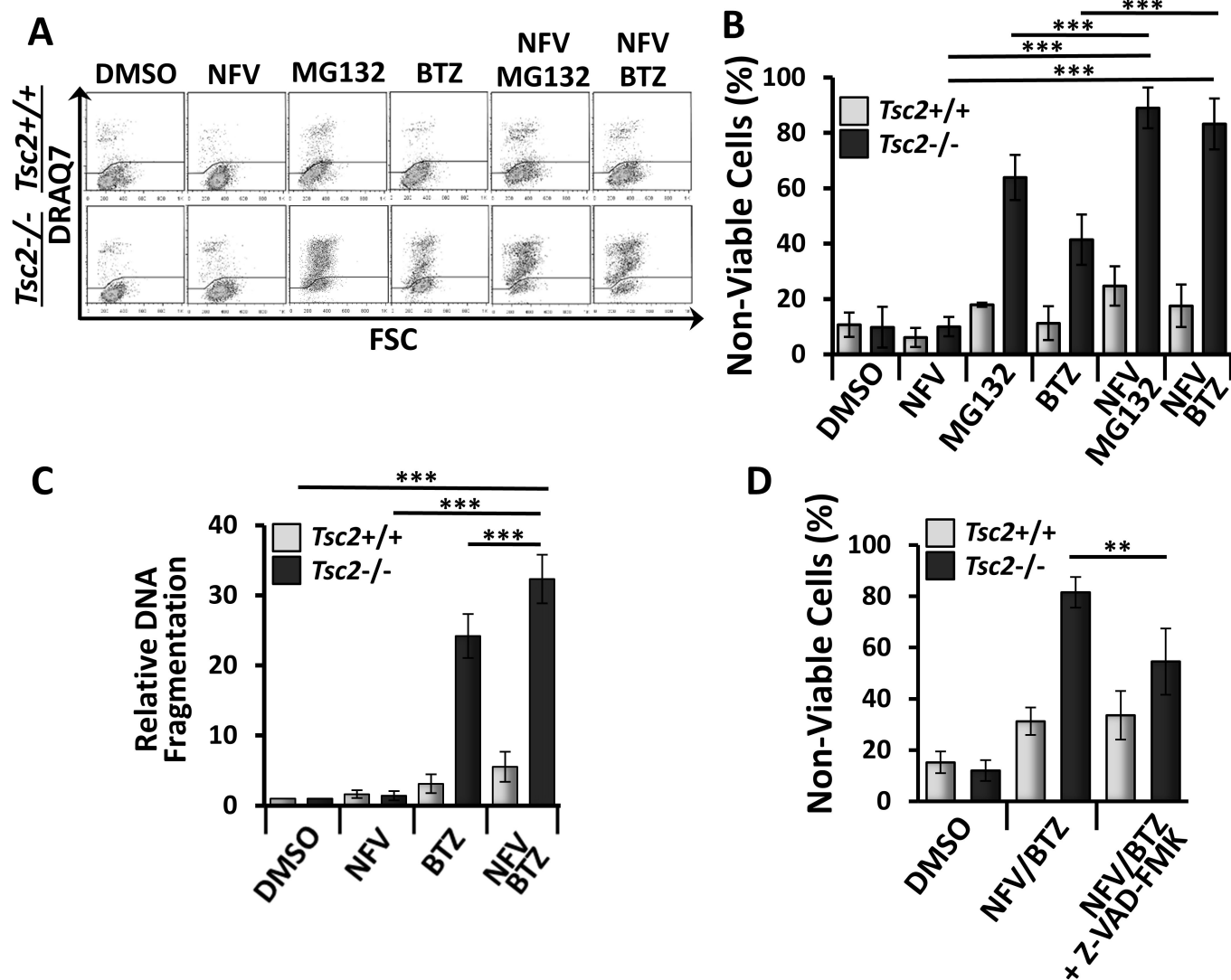
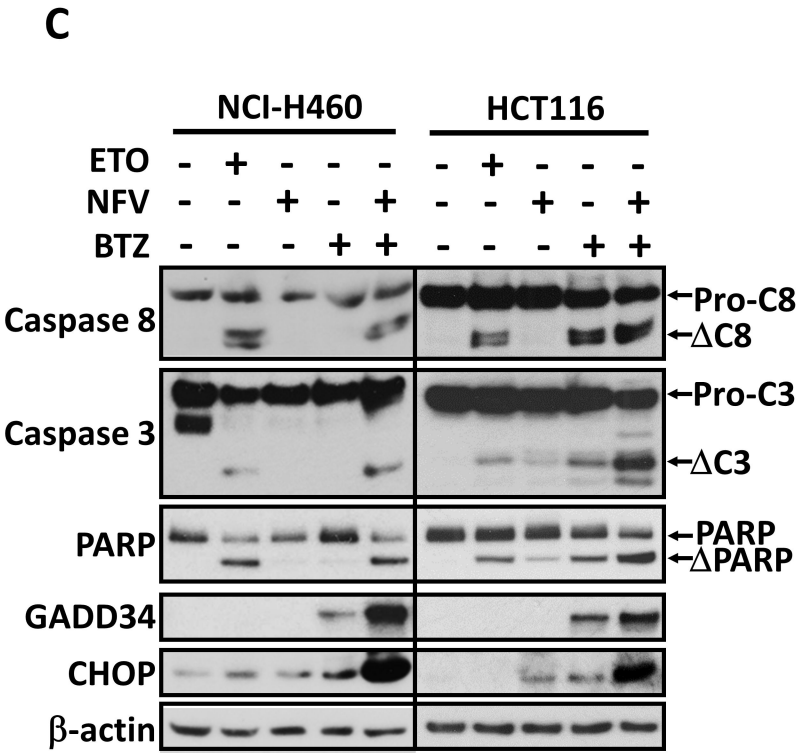
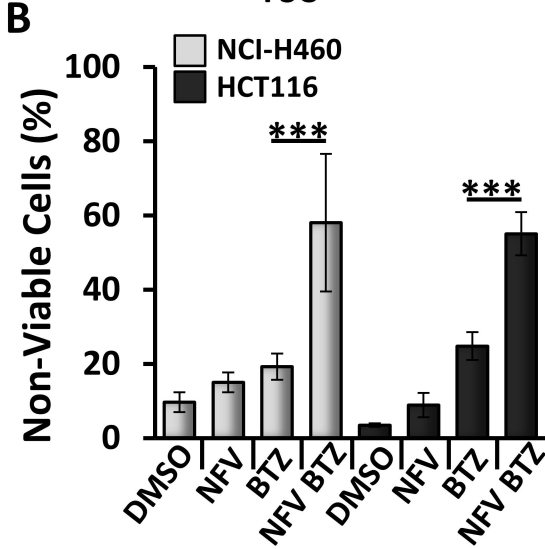
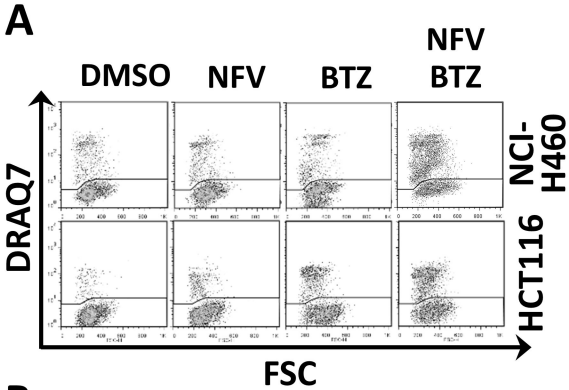


Figure 3



**Figure 4**

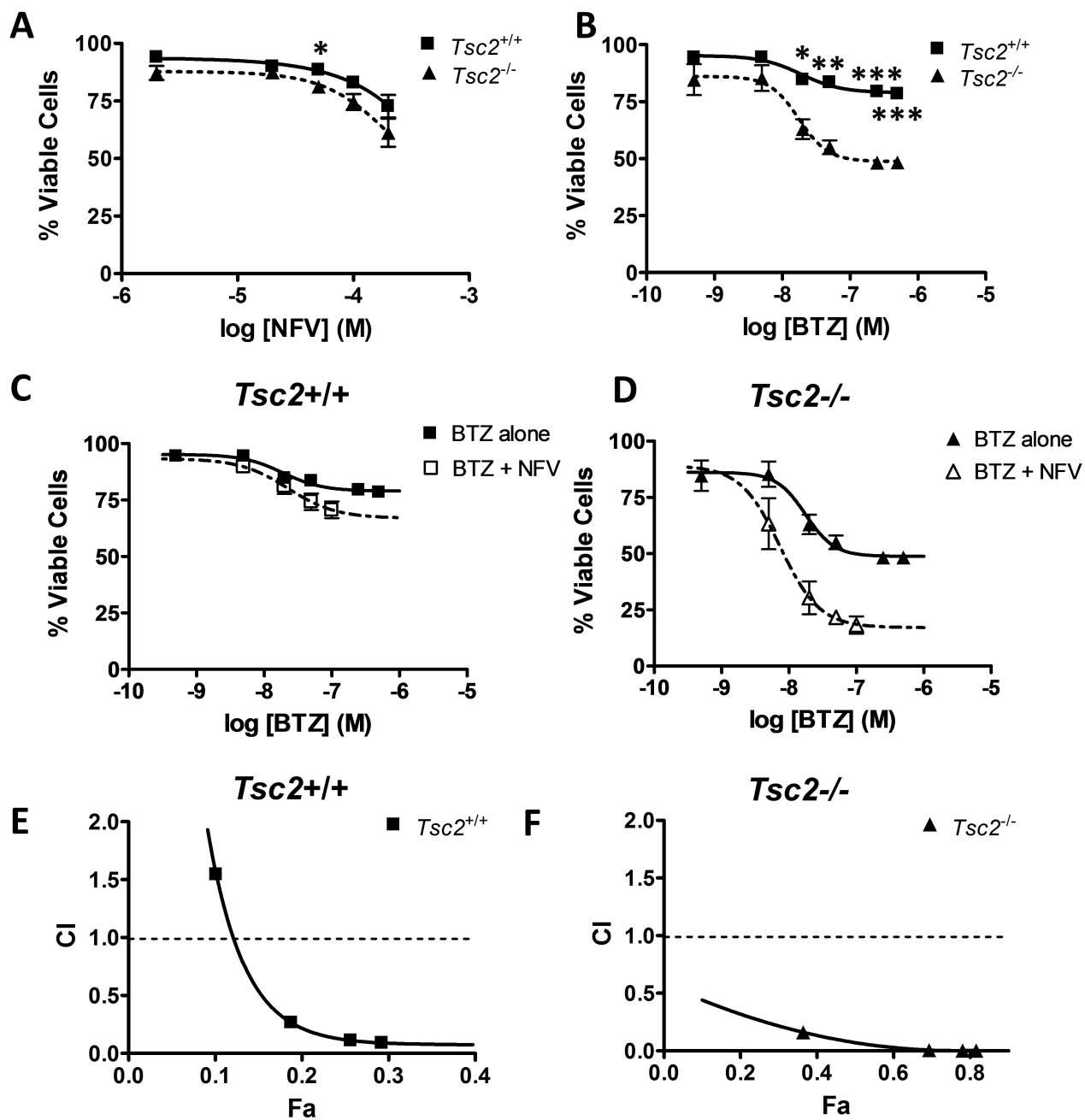
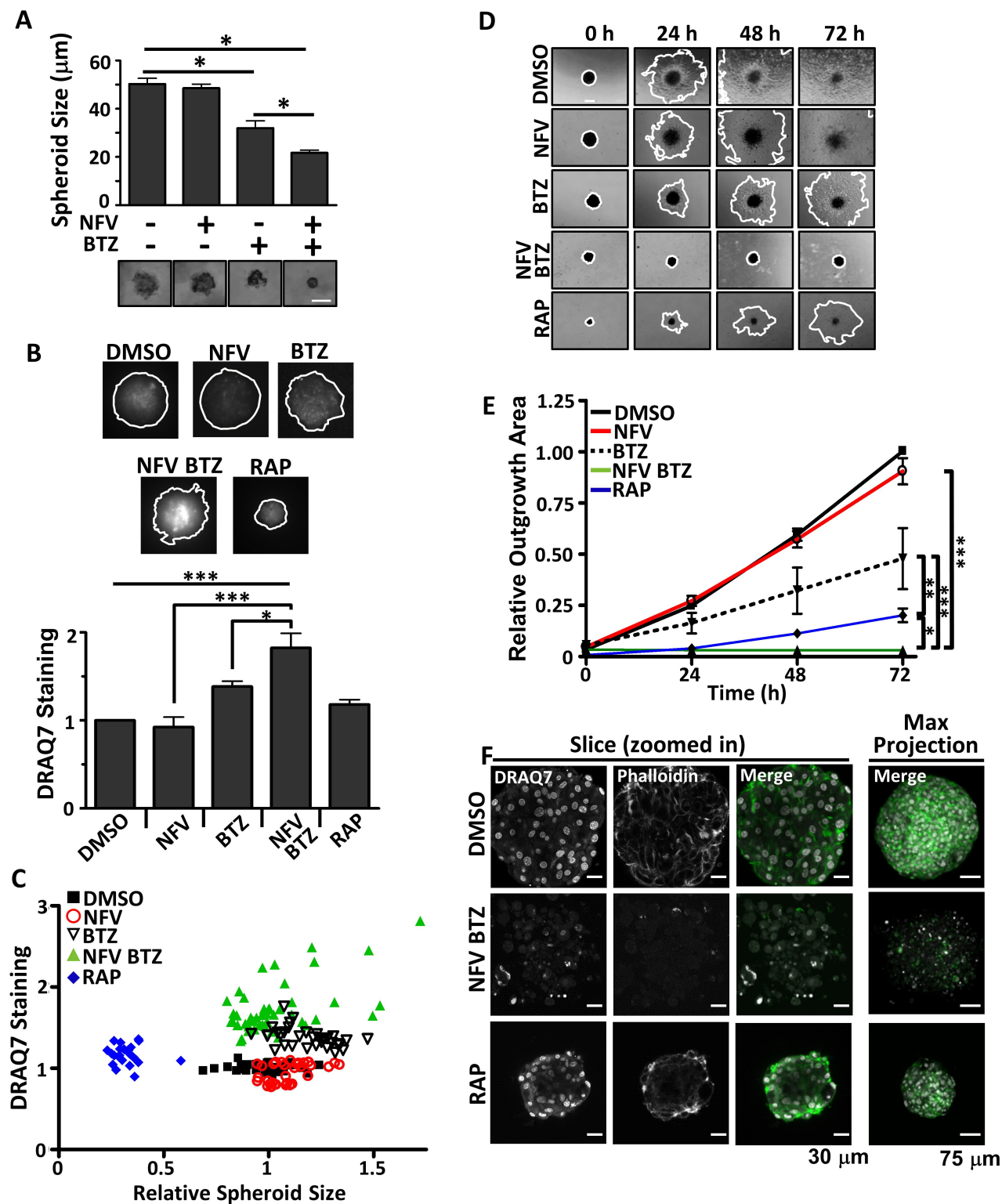


Figure 5



**Figure 6**

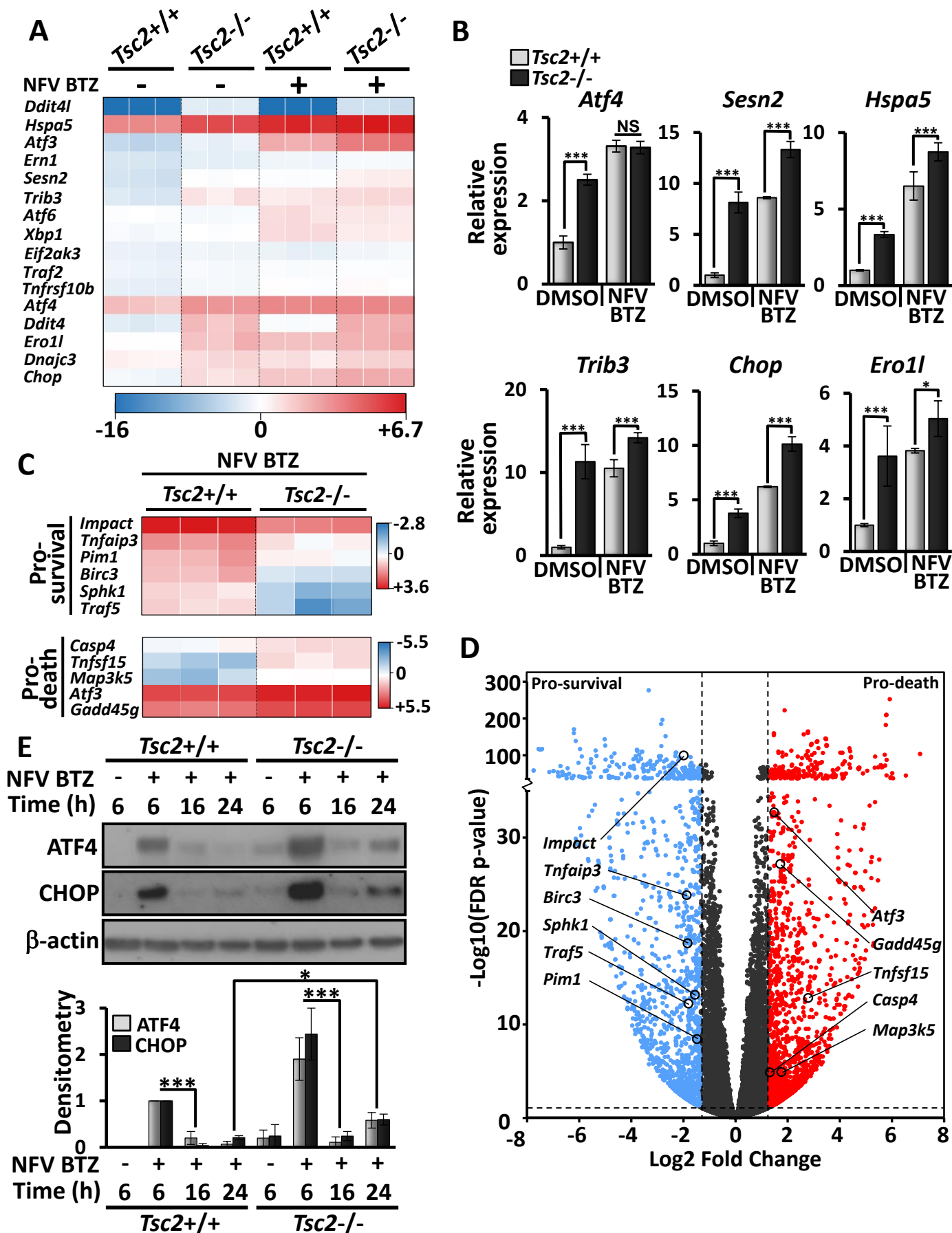
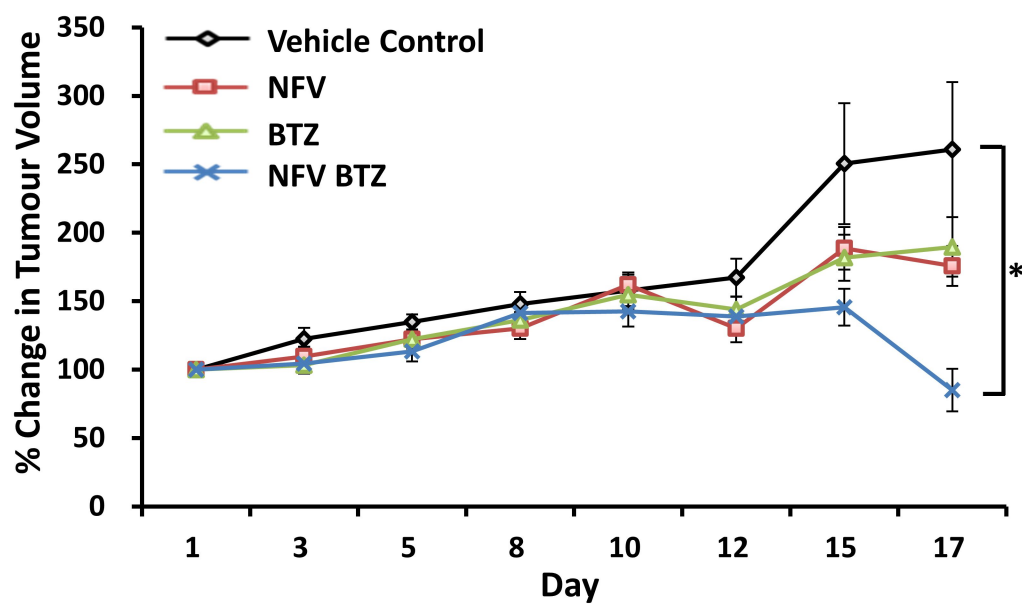
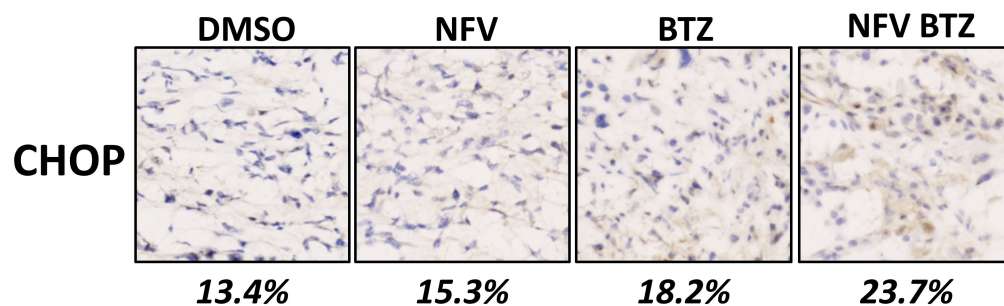


Figure 7

A



B



C

